

Searching for Dark Matter with a Superconducting Qubit

Akash V. Dixit^{1,2,3,*} Srivatsan Chakram,^{1,2,4} Kevin He^{1,2} Ankur Agrawal^{1,2,3} Ravi K. Naik^{1,2,3,5}
David I. Schuster,^{1,2,6} and Aaron Chou⁷

¹James Franck Institute, University of Chicago, Chicago, Illinois 60637, USA

²Department of Physics, University of Chicago, Chicago, Illinois 60637, USA


³Kavli Institute for Cosmological Physics, University of Chicago, Chicago, Illinois 60637, USA

⁴Department of Physics and Astronomy, Rutgers University, Piscataway, New Jersey 08854, USA

⁵Department of Physics, University of California Berkeley, Berkeley, California 94720, USA

⁶Pritzker School of Molecular Engineering, University of Chicago, Chicago, Illinois 60637, USA

⁷Fermi National Accelerator Laboratory, Batavia, Illinois 60510, USA

 (Received 19 October 2020; revised 5 February 2021; accepted 22 February 2021; published 8 April 2021)

Detection mechanisms for low mass bosonic dark matter candidates, such as the axion or hidden photon, leverage potential interactions with electromagnetic fields, whereby the dark matter (of unknown mass) on rare occasion converts into a single photon. Current dark matter searches operating at microwave frequencies use a resonant cavity to coherently accumulate the field sourced by the dark matter and a near standard quantum limited (SQL) linear amplifier to read out the cavity signal. To further increase sensitivity to the dark matter signal, sub-SQL detection techniques are required. Here we report the development of a novel microwave photon counting technique and a new exclusion limit on hidden photon dark matter. We operate a superconducting qubit to make repeated quantum nondemolition measurements of cavity photons and apply a hidden Markov model analysis to reduce the noise to 15.7 dB below the quantum limit, with overall detector performance limited by a residual background of real photons. With the present device, we perform a hidden photon search and constrain the kinetic mixing angle to $\epsilon \leq 1.68 \times 10^{-15}$ in a band around 6.011 GHz (24.86 μeV) with an integration time of 8.33 s. This demonstrated noise reduction technique enables future dark matter searches to be sped up by a factor of 1,300. By coupling a qubit to an arbitrary quantum sensor, more general sub-SQL metrology is possible with the techniques presented in this Letter.

DOI: [10.1103/PhysRevLett.126.141302](https://doi.org/10.1103/PhysRevLett.126.141302)

Introduction.—The nature of dark matter is an enduring mystery of our Universe. Observations of galaxy rotation curves, gravitational lensing, and the presence of structure in the cosmos all inform our understanding of dark matter, but provide little insight into its intrinsic properties [1,2]. Though the gravitational evidence for the existence of dark matter is extensive [2], thus far, dark matter has evaded direct detection in terrestrial experiments. We are interested in testing the hypothesis that dark matter is composed of waves of low mass bosons, which due to their high galactic phase space density, arrive as coherent waves with macroscopic occupation number. Well-known dark matter candidates include the axion and hidden sector photon, which both have compelling cosmological origin stories [3–7].

One method for detecting these dark matter waves exploits their interactions with the electromagnetic field

[7,8]. A microwave cavity with resonance frequency tuned to the mass of the hypothetical particle is used to coherently accumulate the electromagnetic response (see Supplemental Material [9]). On rare occasions, the dark matter deposits a single photon in the cavity.

There are specified targets in the parameter space of coupling and dark matter mass in the case of the axion of quantum chromodynamics (QCD). The expected signal photon occupation number is $\sim 10^{-2}$ for searches like the Axion Dark Matter eXperiment operating at 650 MHz [10]. However, for searches at higher frequencies, the microwave cavity volume must shrink to maintain the resonance condition. The signal photon rate scales with the volume of the cavity, making detection of smaller signals increasingly challenging at higher frequencies. For an axion search with the microwave cavity (6.011 GHz) used in the present Letter and given the experimental parameters in typical axion search experiments [11–14], QCD axion models [15–18] predict a signal with mean photon number of $\bar{n}_{\text{axion}} \sim 10^{-8} - 10^{-5}$ per measurement. For hidden photons, the parameter space is less constrained [6,19,20], and the mean photon number per measurement could be

Published by the American Physical Society under the terms of the [Creative Commons Attribution 4.0 International license](https://creativecommons.org/licenses/by/4.0/). Further distribution of this work must maintain attribution to the author(s) and the published article's title, journal citation, and DOI. Funded by SCOAP³.

$\bar{n}_{\text{HP}} \leq 10^{-1}$. Currently, these searches employ linear amplification operating near the standard quantum limit (SQL) [21] to read out the built up signal in the microwave cavity, where the noise variance is equivalent to fluctuations of an effective background of $\bar{n}_{\text{SQL}} = 1$. At gigahertz frequencies and above, the noise inherent to quantum limited linear amplification overwhelms the signal, making the search untenable ($\bar{n}_{\text{SQL}} \gg \bar{n}_{\text{axion}}, \bar{n}_{\text{HP}}$).

We use single-photon resolving detectors to avoid quantum noise by measuring only field amplitude, resulting in insensitivity to the conjugate phase observable. The noise is then dominated by the Poisson fluctuations of the background counts and ultimately limited by the shot noise of the signal itself [22]. Superconducting nanowire single-photon detectors or photomultiplier tubes can readily count infrared photons; however, these technologies are not well suited to detect single low energy microwave photons [23]. Here, we develop a detector that is sensitive in the microwave regime and has a low dark count probability commensurate with the small signal rates expected in a dark matter experiment.

Qubit-based photon counter.—In order to construct a single-photon counter, we employ quantum nondemolition (QND) techniques pioneered in atomic physics [24,25]. To count photons, we utilize the interaction between a superconducting transmon qubit [26,27] and the field in a microwave cavity, as described by the Jaynes-Cummings Hamiltonian [28] in the dispersive limit (qubit-cavity coupling \ll qubit, cavity detuning): $\mathcal{H}/\hbar = \omega_c a^\dagger a + \frac{1}{2} \omega_q \sigma_z + 2\chi a^\dagger a \frac{1}{2} \sigma_z$. The Hamiltonian can be recast to elucidate a key feature: a photon-number-dependent frequency shift (2χ) of the qubit transition [Fig. 1(b)],

$$\mathcal{H}/\hbar = \omega_c a^\dagger a + \frac{1}{2} (\omega_q + 2\chi a^\dagger a) \sigma_z. \quad (1)$$

We use an interferometric Ramsey measurement of the qubit frequency to infer the cavity state [30]. Errors in the measurement occur due to qubit decay, dephasing, heating,

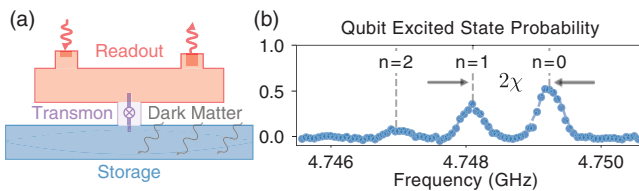


FIG. 1. Superconducting transmon qubit dispersively coupled to high Q storage cavity. (a) Schematic of photon counting device consisting of storage and readout cavities bridged by a transmon qubit [29]. The interaction between the dark matter and electromagnetic field results in a photon being deposited in the storage cavity. (b) Qubit spectroscopy reveals that the storage cavity population is imprinted as a shift of the qubit transition frequency. The photon-number-dependent shift is 2χ per photon.

cavity decay, and readout infidelity, introducing inefficiencies or, worse, false positive detections. For contemporary transmon qubits, these errors occur with much greater probability (1%–10%) than the appearance of a dark matter induced photon, resulting in a measurement that is limited by detector errors. The qubit-cavity interaction ($2\chi a^\dagger a \frac{1}{2} \sigma_z$) is composed solely of number operators and commutes with the bare Hamiltonian of the cavity ($\omega_c a^\dagger a$) and qubit ($\frac{1}{2} \omega_q \sigma_z$). Thus, the cavity state collapses to a Fock state ($|0\rangle$ or $|1\rangle$ in the $\bar{n} \ll 1$ limit) upon measurement, rather than being absorbed and destroyed [31–34]. Repeated measurements of the cavity photon number made via this QND operator enable us to devise a counting protocol, shown in Fig. 2(a), insensitive to errors in any individual measurement [35–37]. This provides exponential rejection of false positives with only a linear cost in measurement time.

In this Letter, we use a device composed of a high quality factor ($Q_s = 2.06 \times 10^7$) 3D cavity [38,39] used to accumulate and store the signal induced by the dark matter (storage, $\omega_s = 2\pi \times 6.011$ GHz), a superconducting transmon qubit ($\omega_q = 2\pi \times 4.749$ GHz), and a 3D cavity strongly coupled to a transmission line ($Q_r = 1.5 \times 10^4$) used to quickly read out the state of qubit (readout, $\omega_r = 2\pi \times 8.052$ GHz) [Fig. 1(a)]. We mount the device to the base stage of a dilution refrigerator at 8 mK.

To count photons, we repeatedly map the cavity population onto the qubit state by performing a cavity number parity measurement with Ramsey interferometry, as depicted in Fig. 2(a). We place the qubit, initialized either in $|g\rangle$ or $|e\rangle$, in a superposition state $1/\sqrt{2}(|g\rangle \pm |e\rangle)$ with a $\pi/2$ pulse. The qubit state precesses at a rate of $|2\chi| = 2\pi \times 1.13$ MHz when there is one photon in the storage cavity due to the photon-dependent qubit frequency shift. Waiting for a time $t_p = \pi/|2\chi|$ results in the qubit state accumulating a π phase if there is one photon in the cavity. We project the qubit back onto the z axis, with a $-\pi/2$ pulse completing the mapping of the storage cavity photon number onto the qubit state. We then determine the qubit state using its standard dispersive coupling to the readout resonator. For weak cavity displacements ($\bar{n} \ll 1$), this protocol functions as a qubit π pulse conditioned on the presence of a single cavity photon [30]. If there are zero photons in the cavity, the qubit remains in its initial state. If there is one photon in the cavity, the qubit state is flipped ($|g\rangle \leftrightarrow |e\rangle$). More generally, this protocol is sensitive to any cavity state with odd photon number population.

Hidden Markov model analysis.—In order to account for all possible error mechanisms during the measurement protocol, we model the evolution of the cavity, qubit, and readout as a hidden Markov process, where the cavity and qubit states are hidden variables that emit as a readout signal [see Fig. 2(b)]. The Markov chain is characterized by the transition matrix (T) [Eq. (2)] that governs how the joint

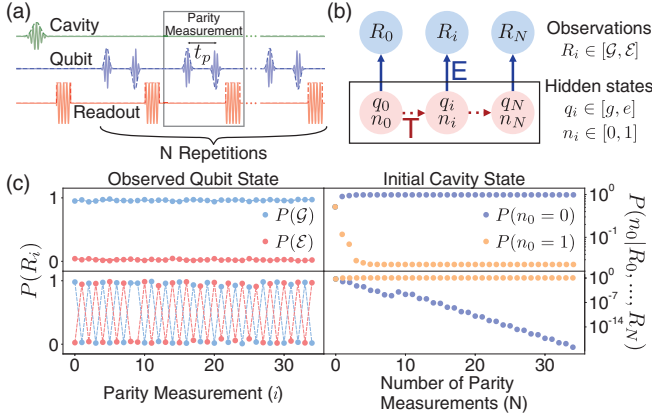


FIG. 2. Photon counting protocol and hidden Markov model analysis. (a) Pulse sequence for photon counting includes cavity initialization and repeated parity measurements, consisting of a $\pi/2$ pulse, a wait time of t_p , and a $-\pi/2$ pulse followed by a qubit readout. (b) Cavity and qubit states evolve under transition matrix T , readout measurements are governed by emission matrix E . (c) Left: sequence of qubit readout signals for two events. Right: reconstructed initial cavity state probabilities. We observe an exponential suppression of the detector error-based false positive probability.

cavity, qubit hidden state $s \in [|0g\rangle, |0e\rangle, |1g\rangle, |1e\rangle]$ evolve, and the emission matrix (E) [Eq. (3)], which determines the probability of a readout signal $R \in [\mathcal{G}, \mathcal{E}]$ given a possible hidden state.

The transition matrix captures the possible qubit and cavity state changes. Qubit (cavity) relaxation $|e\rangle \rightarrow |g\rangle$ ($|1\rangle \rightarrow |0\rangle$) occurs with a probability $P_{eg}^\downarrow = 1 - e^{-t_m/T_1^q}$ ($P_{10} = 1 - e^{-t_m/T_1^i}$). The probability of spontaneous heating $|g\rangle \rightarrow |e\rangle$ ($|0\rangle \rightarrow |1\rangle$) of the qubit (cavity) toward its steady-state population is given by $P_{ge}^\uparrow = \bar{n}_q [1 - e^{-t_m/T_1^q}]$ ($P_{01} = \bar{n}_c [1 - e^{-t_m/T_1^i}]$). \bar{n}_c is set to zero in the model in order to penalize events in which a photon appears in the cavity after the measurement sequence has begun. This makes the detector insensitive to cavity heating events. Dephasing during the parity measurement occurs with probability $P^\phi = 1 - e^{-t_p/T_2^q}$, leading to outcomes indistinguishable from qubit heating or decay. The transition matrix contains all qubit errors: $P_{ge} = P_{ge}^\uparrow + P^\phi$ and $P_{eg} = P_{eg}^\downarrow + P^\phi$. P_{gg} , P_{ee} , P_{00} , and P_{11} correspond to events where no error occurs, such that probabilities pairwise sum to unity (e.g., $P_{gg} + P_{ge} = 1$). These probabilities are calculated using independently measured qubit coherences ($T_1^q = 108 \pm 18 \mu\text{s}$, $T_2^q = 61 \pm 4 \mu\text{s}$), cavity lifetime ($T_1^s = 546 \pm 23 \mu\text{s}$), qubit spurious excited state population ($\bar{n}_q = 5.1 \pm 0.3 \times 10^{-2}$), the length of the parity measurement ($t_p = 380 \text{ ns}$), and the time between parity measurements ($t_m = 10 \mu\text{s}$) (see Supplemental Material [9] for descriptions of experimental protocols used to determine these parameters [40–44]). The repetition rate of the experiment is constrained primarily by the

readout time ($3 \mu\text{s}$) and time for the readout resonator to relax back to the ground state

$$T = \begin{bmatrix} |0g\rangle & |0e\rangle & |1g\rangle & |1e\rangle \\ P_{00}P_{gg} & P_{00}P_{ge} & P_{01}P_{ge} & P_{01}P_{gg} \\ P_{00}P_{eg} & P_{00}P_{ee} & P_{01}P_{ee} & P_{01}P_{eg} \\ P_{10}P_{gg} & P_{10}P_{ge} & P_{11}P_{ge} & P_{11}P_{gg} \\ P_{10}P_{eg} & P_{10}P_{ee} & P_{11}P_{ee} & P_{11}P_{eg} \end{bmatrix} \begin{bmatrix} |0g\rangle \\ |0e\rangle \\ |1g\rangle \\ |1e\rangle \end{bmatrix}. \quad (2)$$

The elements of the emission matrix are composed of the readout fidelities of the ground and excited states of the qubit ($F_{g\mathcal{G}} = 95.8 \pm 0.4\%$, $F_{e\mathcal{E}} = 95.3 \pm 0.5\%$). Noise from the first stage cryogenic HEMT amplifier sets the readout fidelity

$$E = \frac{1}{2} \begin{bmatrix} \mathcal{G} & \mathcal{E} \\ F_{g\mathcal{G}} & F_{g\mathcal{E}} \\ F_{e\mathcal{G}} & F_{e\mathcal{E}} \\ F_{g\mathcal{G}} & F_{g\mathcal{E}} \\ F_{e\mathcal{G}} & F_{e\mathcal{E}} \end{bmatrix} \begin{bmatrix} |0g\rangle \\ |0e\rangle \\ |1g\rangle \\ |1e\rangle \end{bmatrix}. \quad (3)$$

Given a set of $N + 1$ measured readout signals (R_0, R_1, \dots, R_N), we reconstruct the initial cavity state probabilities $P(n_0 = 0)$ and $P(n_0 = 1)$ by using the backward algorithm [Eq. (4)] [35,36] and summing over all possible initial qubit states.

$$P(n_0) = \sum_{s_0 \in \{|n_0, g\rangle, |n_0, e\rangle\}} \sum_{s_1} \cdots \sum_{s_N} E_{s_0, R_0} T_{s_0, s_1} E_{s_1, R_1} \cdots T_{s_{N-1}, s_N} E_{s_N, R_N}. \quad (4)$$

This reconstruction includes terms corresponding to all the possible processes that could occur. For example, a readout measurement of \mathcal{G} followed by \mathcal{E} could occur due to the correct detection of a photon in the cavity (with probability $P_{11}P_{gg}F_{e\mathcal{E}}/2$). Alternatively, this measurement could be produced by a qubit heating event ($P_{00}P_{ge}F_{e\mathcal{E}}/2$) or a readout error ($P_{00}P_{gg}F_{g\mathcal{E}}/2$). Figure 2(c) displays the measured readout signals and reconstructed initial cavity probabilities of two events. The top panels correspond to the absence of a cavity photon and the bottom panels indicate the presence of a photon.

We apply a likelihood ratio test to the reconstructed cavity state probabilities to determine if the cavity contained zero or one photon $\{\lambda = [P(n_0 = 1)]/[P(n_0 = 0)]\}$. If the likelihood ratio is greater than (less than) a threshold, $\lambda > \lambda_{\text{thresh}}$ ($\lambda \leq \lambda_{\text{thresh}}$), we determine the cavity to contain one (zero) photon. The probability of a detector error induced false positive is therefore less than $1/(\lambda_{\text{thresh}} + 1)$. As the threshold for detection increases, so too does the number of repeated parity measurements needed to confirm the presence of a photon, exacting a cost to detection

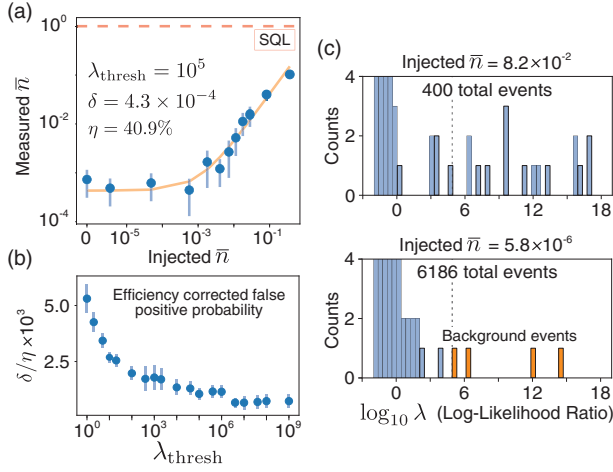


FIG. 3. Detector characterization. (a) After a variable initial cavity displacement, 30 repeated parity measurements of cavity photon state are performed and a threshold λ_{thresh} is applied to determine the cavity population. Detector efficiency (η) and false positive probability (δ) are determined from the fit in orange. The dashed red line corresponds to the standard quantum limit, which results in the noise equivalent of one photon occupation. (b) The efficiency corrected false positive probability (δ/η) vs threshold (λ_{thresh}) curve asymptotes at high thresholds, indicating qubit errors are now a subdominant contribution to the total detector false positive probability. (c) Histograms of log-likelihood ratios of all events for two different injected mean photon numbers. The histogram y axis is cut off at four counts to view the rare events at high log-likelihood ratios. The dashed gray line corresponds to $\lambda_{\text{thresh}} = 10^5$ used in (a). The unexpected photon events when very small photon numbers are injected with log-likelihood ratios are from a photon background occupying the storage cavity rather than detector error-based false positives.

efficiency that is linear in the number of measurements. More importantly, for the detection of rare events, false positives are exponentially suppressed with more repeated measurements, as evident in Fig. 2(c).

Detector characterization.—To characterize the detector, we populate the cavity by applying a weak drive ($\bar{n} \ll 1$). We map out the relationship between the probability of injected and measured photons [Fig. 3(a)] by varying the injected mean photon population ($\bar{n} = \alpha^2$), performing 30 repeated parity measurements, and applying λ_{thresh} to discriminate between one and zero photon events. We fit this relationship with the function $\bar{n}_{\text{meas}} = \eta \bar{n}_{\text{inj}} + \delta$. We obtain the efficiency of detection $\eta = 0.409 \pm 0.055$ and the false positive probability $\delta = 4.3 \pm 1.1 \times 10^{-4}$ at threshold $\lambda_{\text{thresh}} = 10^5$ with goodness of fit $\chi^2_{\text{fit}} = 0.0048$.

Figure 3(b) shows that the efficiency corrected false positive probability (δ/η) initially decreases for low-likelihood thresholds λ_{thresh} , indicating a suppression of qubit and readout-based false positives. Leveling off at larger thresholds indicates that the dominant source of false positives is no longer detector errors, but rather a background of real photons.

False positives that occur when qubit errors are highly suppressed (at large λ_{thresh}) are due to a photon background in the storage cavity. In experiments with no photons injected into the cavity, we observe events with high-likelihood ratios comparable with those seen in experiments with injected photons [Fig. 3(c)]. The detector thus correctly identifies real photons that set the background for dark matter searches. We measure the background cavity occupation to be $\bar{n}_c = 7.3 \pm 2.9 \times 10^{-4}$, corresponding to a temperature of 39.9 ± 2.2 mK.

Because the measured cavity photon temperature is greater than the physical 8 mK temperature of the device there must be coupling to extraneous baths. One contribution, arising from coupling to quasiparticles via qubit dressing of the cavity [45], results in a photon population of $\bar{n}_c^q = 1.8 \pm 0.1 \times 10^{-4}$ (see Supplemental Material [9]). Suppression of quasiparticle production could be achieved by enhanced infrared filtering, extensive radiation shielding, gap engineering, and quasiparticle trapping [46–48]. Other sources of background photons could include blackbody radiation from higher temperature stages of the dilution refrigerator, poorly thermalized or insufficiently attenuated microwave lines, or amplifier noise [49,50].

Hidden photon dark matter exclusion.—By counting photons with repeated parity measurements and applying a Markov-model-based analysis, we demonstrate single-photon detection with background shot noise reduced to $-10 \log_{10} \sqrt{\bar{n}_c} = 15.7 \pm 0.9$ dB below the quantum limit. We use this detection technique to conduct a narrow band hidden photon search. We collect 15,141 independent measurements where the injected \bar{n} is well below the background population \bar{n}_c and the time between measurements is much longer than either cavity or qubit timescale. Each measurement consists of integrating the signal (for the cavity lifetime, $T_1^s = 546 \mu\text{s}$) and counting the number of photons in the cavity with 30 repeated parity measurements ($30 \times t_m = 300 \mu\text{s}$). The total search time is $15,141 \times (546 + 300) \mu\text{s} = 12.81$ s with a duty cycle of $546 \mu\text{s}/846 \mu\text{s} = 65\%$ (8.33 s of integration). We apply a detection threshold of $\lambda_{\text{thresh}} = 10^5$, such that the qubit and readout errors are suppressed below the background photon probability ($1/(\lambda_{\text{thresh}} + 1) < \bar{n}_c$). We count 9 photons in 15,141 measurements. Accounting for the systematic uncertainties of the experiment (statistical uncertainties are dominant, see Supplemental Material [9] for full treatment of all systematics [51,52]), a hidden photon candidate on resonance with the storage cavity ($m_\nu c^2 = \hbar \omega_s$), with mixing angle $\epsilon > 1.68 \times 10^{-15}$ is excluded at the 90% confidence level. Figure 4 shows the regions of hidden photon parameter space excluded by the qubit-based search, assuming the hidden photon comprises all the dark matter density ($\rho_{\text{DM}} = 0.4 \text{ GeV}/\text{cm}^3$). The detector is maximally sensitive to dark matter candidates with masses within a narrow window around the resonance frequency of the cavity. This window is set by

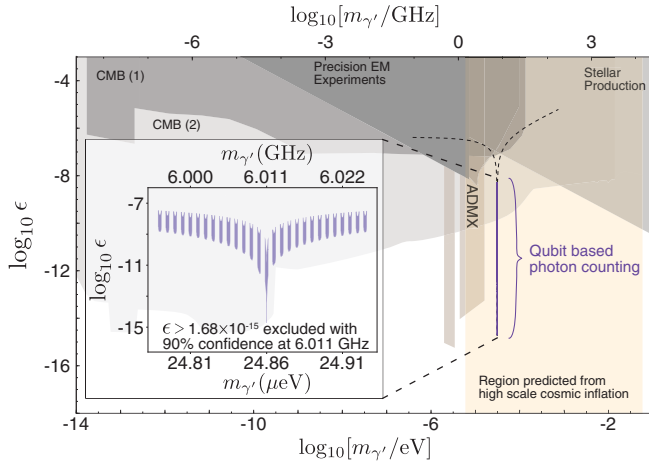


FIG. 4. Hidden photon dark matter parameter space. Shaded regions in the hidden photon parameter space [6,55] of coupling (ϵ) and mass (m_γ) are excluded. In the orange band, hidden photon dark matter is naturally produced in models of high scale cosmic inflation [7]. The exclusion set with the qubit-based photon counting search presented in this Letter is shown in purple (dashed black line to guide the eye). On resonance with the storage cavity ($m_\gamma c^2 = \hbar\omega_s$), the hidden photon kinetic mixing angle is constrained to $\epsilon \leq 1.68 \times 10^{-15}$ with 90% confidence. The Ramsey measurement procedure is also sensitive to signals that produce cavity states with odd photon number populations greater than the measured background. Sensitivity to off-resonant candidates gives rise to bands of exclusion (see inset) centered around regions where the photon-number-dependent qubit frequency shift is an odd multiple of 2χ [54]. Sensitivity to large amplitude and highly detuned signals is limited by the bandwidth of the $\pi/2$ pulses used in the parity measurements.

the line shape of the dark matter [53] ($Q_{\text{DM}} \sim 10^6$) such that the sensitivity falls to half the maximum (-3 dB point) 3 kHz away from the cavity resonance. Additionally, sensitivity to off-resonant candidates occurs in regions where the photon-number-dependent qubit shift is an odd multiple of the dispersive shift 2χ (see Supplemental Material [9] for calculation of hidden photon constraints [54]).

Conclusions.—Photon number measurements allow us to gain unprecedented sensitivity to dark matter signals. The single-photon counting protocol demonstrated in this Letter results in a 15.7 dB metrological gain, relative to the SQL. This improvement is currently limited by background photons $\bar{n}_c = 7.3 \times 10^{-4}$ whose suppression by improved filtering and shielding will further increase detector sensitivity.

In a full scale dark matter search, where the cavity is tuned to scan a wide range of dark matter masses, it is possible to estimate and subtract the background population of the cavity. The standard technique is to measure the photon population as the cavity is tuned to neighboring cavity frequencies separated by more than the dark matter linewidth. The signal hypothesis can be tested by repeating the experiment with an auxiliary cavity of the same frequency as the detection cavity, but with poor coupling to the dark matter.

The integration time required for a background limited dark matter search is determined by the signal rate ($R_s = \bar{n}_{\text{DM}}/T_1^s$) and background rate ($R_b = \bar{n}_c/T_1^s$): $R_s t > \sqrt{R_b t}$. The signal integration time scales with the background photon probability: $t > \bar{n}_c T_1^s / \bar{n}_{\text{DM}}^2$. The photon detection technique developed in this Letter constitutes a $\bar{n}_{\text{SQL}}/\bar{n}_c \sim 1,300$ times speed up of dark matter searches, relative to a linear quantum limited amplifier.

This unprecedented sensitivity enables future cavity-based searches for axions and hidden photons in the 3–30 GHz range. At lower frequencies, thermal backgrounds will dominate and at higher frequencies, near the aluminium Josephson junction plasma frequency, qubit losses will degrade the measurement. A fixed frequency qubit can be coupled to a tunable cavity to scan over a dark matter mass range of order $\mathcal{O}(\text{GHz})$, limited by the tuning range of the cavity. As long as the photon-number-dependent shift 2χ is resolvable and the qubit and cavity are sufficiently detuned at each tuning, the QND counting protocol can be harnessed to perform a search with sub-SQL noise. A non-linear element made of higher T_c superconductor, such as tantalum [56], niobium, or titanium nitride, could be used to access frequencies beyond 30 GHz (see Supplemental Material [9] for more information about future dark matter searches [57–62]).

High fidelity nondestructive photon counting can be utilized for accurate primary thermometry in low temperature microwave systems. This technique is applicable to quantum computing architectures that utilize long-lived storage cavities [63,64]. Assessing the residual cavity population independently of the qubit errors allows for both single shot and real time monitoring of the storage cavity, crucial when preparing states whose fidelity is sensitive to the initial conditions.

In this Letter, we demonstrate a state-of-the-art photon counter for dark matter sensing. More generally, this technique of performing many QND measurements within a mode resolution time can be used to perform sub-SQL metrology in other quantum sensing applications.

We thank N. Earnest, A. Oriani, and C. Hann for discussions. We gratefully acknowledge the support provided by the Heising-Simons Foundation. This work made use of the Pritzker Nanofabrication Facility of the Institute for Molecular Engineering at the University of Chicago, which receives support from Soft and Hybrid Nanotechnology Experimental (SHyNE) Resource (NSF ECCS-1542205), a node of the National Science Foundations National Nanotechnology Coordinated Infrastructure. This manuscript has been authored by Fermi Research Alliance, LLC under Contract No. DEAC02-07CH11359 with the U.S. Department of Energy, Office of Science, Office of High Energy Physics, with support from its QuantISED program. We acknowledge support from the Samsung Advanced Institute of Technology Global Research Partnership.

- *avdixit@uchicago.edu
- [1] M. Tanabashi, K. Hagiwara, K. Hikasa, K. Nakamura, Y. Sumino, F. Takahashi, J. Tanaka, K. Agashe, G. Aielli, C. Amsler *et al.* (Particle Data Group), Review of particle physics, *Phys. Rev. D* **98**, 030001 (2018).
 - [2] V. C. Rubin, W. K. Ford Jr., and N. Thonnard, Rotational properties of 21 SC galaxies with a large range of luminosities and radii, from NGC 4605 ($R = 4$ kpc) to UGC 2885 ($R = 122$ kpc), *Astrophys. J.* **238**, 471 (1980).
 - [3] J. Preskill, M. B. Wise, and F. Wilczek, Cosmology of the invisible axion, *Phys. Lett.* **120B**, 127 (1983).
 - [4] L. Abbott and P. Sikivie, A cosmological bound on the invisible axion, *Phys. Lett.* **120B**, 133 (1983).
 - [5] M. Dine and W. Fischler, The not so harmless axion, *Phys. Lett.* **120B**, 137 (1983).
 - [6] P. Arias, D. Cadamuro, M. Goodsell, J. Jaeckel, J. Redondo, and A. Ringwald, WISPy cold dark matter, *J. Cosmol. Astropart. Phys.* **06** (2012) 013.
 - [7] P. W. Graham, J. Mardon, and S. Rajendran, Vector dark matter from inflationary fluctuations, *Phys. Rev. D* **93**, 103520 (2016).
 - [8] P. Sikivie, Experimental Tests of the “Invisible” Axion, *Phys. Rev. Lett.* **51**, 1415 (1983).
 - [9] See Supplemental Material at <http://link.aps.org/supplemental/10.1103/PhysRevLett.126.141302> for discussion of the device fabrication, experiment calibration, data analysis, and dark matter exclusion calculations.
 - [10] N. Du, N. Force, R. Khatiwada, E. Lentz, R. Ottens *et al.*, Search for Invisible Axion Dark Matter with the Axion Dark Matter Experiment, *Phys. Rev. Lett.* **120**, 151301 (2018).
 - [11] T. Braine, R. Cervantes, N. Crisosto, N. Du, S. Kimes, L. Rosenberg, G. Rybka, J. Yang, D. Bowring, A. Chou *et al.*, Extended Search for the Invisible Axion with the Axion Dark Matter Experiment, *Phys. Rev. Lett.* **124** (2020).
 - [12] B. M. Brubaker, L. Zhong, Y. V. Gurevich, S. B. Cahn, S. K. Lamoreaux, M. Simanovskaia, J. R. Root, S. M. Lewis, S. Al Kenany, K. M. Backes *et al.*, First Results from a Microwave Cavity Axion Search at $24 \mu\text{eV}$, *Phys. Rev. Lett.* **118**, 061302 (2017).
 - [13] L. Zhong, S. Al Kenany, K. Backes, B. Brubaker, S. Cahn, G. Carosi, Y. Gurevich, W. Kindel, S. Lamoreaux, K. Lehnert *et al.*, Results from phase I of the HAYSTAC microwave cavity axion experiment, *Phys. Rev. D* **97** (2018).
 - [14] K. M. Backes, D. A. Palken, S. A. Kenany, B. M. Brubaker, S. B. Cahn, A. Droster, G. C. Hilton, S. Ghosh, H. Jackson, S. K. Lamoreaux *et al.*, A quantum enhanced search for dark matter axions, *Nature (London)* **590**, 238 (2021).
 - [15] M. Dine, W. Fischler, and M. Srednicki, A simple solution to the strong CP problem with a harmless axion, *Phys. Lett.* **104B**, 199 (1981).
 - [16] A. Zhitnitsky, On Possible Suppression of the Axion Hadron Interactions. (In Russian), *Sov. J. Nucl. Phys.* **31**, 260 (1980).
 - [17] J. E. Kim, Weak-Interaction Singlet and Strong CP Invariance, *Phys. Rev. Lett.* **43**, 103 (1979).
 - [18] M. Shifman, A. Vainshtein, and V. Zakharov, Can confinement ensure natural CP invariance of strong interactions?, *Nucl. Phys.* **B166**, 493 (1980).
 - [19] D. Horns, J. Jaeckel, A. Lindner, A. Lobanov, J. Redondo, and A. Ringwald, Searching for WISPy cold dark matter with a dish antenna, *J. Cosmol. Astropart. Phys.* **04** (2013) 016.
 - [20] S. Chaudhuri, P. W. Graham, K. Irwin, J. Mardon, S. Rajendran, and Y. Zhao, Radio for hidden-photon dark matter detection, *Phys. Rev. D* **92** (2015).
 - [21] C. M. Caves, Quantum limits on noise in linear amplifiers, *Phys. Rev. D* **26**, 1817 (1982).
 - [22] S. K. Lamoreaux, K. A. van Bibber, K. W. Lehnert, and G. Carosi, Analysis of single-photon and linear amplifier detectors for microwave cavity dark matter axion searches, *Phys. Rev. D* **88**, 035020 (2013).
 - [23] R. Hadfield, Single-photon detectors for optical quantum information applications, *Nat. Photonics* **3**, 696 (2009).
 - [24] M. Brune, S. Haroche, V. Lefevre, J. M. Raimond, and N. Zagury, Quantum nondemolition measurement of small photon numbers by Rydberg-atom phase-sensitive detection, *Phys. Rev. Lett.* **65**, 976 (1990).
 - [25] S. Gleyzes, S. Kuhr, C. Guerlin, J. Bernu, S. Deléglise, U. Busk, M. Brune, J.-M. Raimond, and S. Haroche, Observing the quantum jumps of light: Birth and death of a photon in a cavity, *Nature (London)* **446**, 297 (2007).
 - [26] J. Koch, T. M. Yu, J. Gambetta, A. A. Houck, D. I. Schuster, J. Majer, A. Blais, M. H. Devoret, S. M. Girvin, and R. J. Schoelkopf, Charge-insensitive qubit design derived from the Cooper pair box, *Phys. Rev. A* **76** (2007).
 - [27] V. Ambegaokar and A. Baratoff, Tunneling Between Superconductors, *Phys. Rev. Lett.* **10**, 486 (1963).
 - [28] E. T. Jaynes and F. W. Cummings, Comparison of quantum and semiclassical radiation theories with application to the beam maser, *Proc. IEEE* **51**, 89 (1963).
 - [29] P. J. Leek, M. Baur, J. M. Fink, R. Bianchetti, L. Steffen, S. Filipp, and A. Wallraff, Cavity Quantum Electrodynamics with Separate Photon Storage and Qubit Readout Modes, *Phys. Rev. Lett.* **104** (2010).
 - [30] S. Kono, K. Koshino, Y. Tabuchi, A. Noguchi, and Y. Nakamura, Quantum non-demolition detection of an itinerant microwave photon, *Nat. Phys.* **14**, 546 (2018).
 - [31] V. B. Braginsky and F. Y. Khalili, Quantum nondemolition measurements: The route from toys to tools, *Rev. Mod. Phys.* **68**, 1 (1996).
 - [32] G. Nogues, A. Rauschenbeutel, S. Osnaghi, M. Brune, J. Raimond, and S. Haroche, Seeing a single photon without destroying it, *Nature (London)* **400**, 239 (1999).
 - [33] B. R. Johnson, M. D. Reed, a. a. Houck, D. I. Schuster, L. S. Bishop, E. Ginossar, J. M. Gambetta, L. Dicarlo, L. Frunzio, S. M. Girvin, and R. J. Schoelkopf, Quantum non-demolition detection of single microwave photons in a circuit, *Nat. Phys.* **6**, 663 (2010).
 - [34] L. Sun, A. Petrenko, Z. Leghtas, B. Vlastakis, G. Kirchmair, K. M. Sliwa, A. Narla, M. Hatridge, S. Shankar, J. Blumoff *et al.*, Tracking photon jumps with repeated quantum non-demolition parity measurements, *Nature (London)* **511**, 444 (2014).
 - [35] H. Zheng, M. Silveri, R. T. Brierley, S. M. Girvin, and K. W. Lehnert, Accelerating dark-matter axion searches with quantum measurement technology, [arXiv:1607.02529](https://arxiv.org/abs/1607.02529).
 - [36] C. T. Hann, S. S. Elder, C. S. Wang, K. Chou, R. J. Schoelkopf, and L. Jiang, Robust readout of bosonic qubits

- in the dispersive coupling regime, *Phys. Rev. A* **98**, 022305 (2018).
- [37] S. S. Elder, C. S. Wang, P. Reinhold, C. T. Hann, K. S. Chou, B. J. Lester, S. Rosenblum, L. Frunzio, L. Jiang, and R. J. Schoelkopf, High-Fidelity Measurement of Qubits Encoded in Multilevel Superconducting Circuits, *Phys. Rev. X* **10** (2020).
- [38] S. Chakram, A. E. Oriani, R. K. Naik, A. V. Dixit, K. He, A. Agrawal, H. Kwon, and D. I. Schuster, Seamless high-Q microwave cavities for multimode circuit QED, [arXiv:2010.16382](https://arxiv.org/abs/2010.16382).
- [39] C. U. Lei, L. Krayzman, S. Ganjam, L. Frunzio, and R. J. Schoelkopf, High coherence superconducting microwave cavities with indium bump bonding, *Appl. Phys. Lett.* **116**, 154002 (2020).
- [40] M. Pechal, L. Huthmacher, C. Eichler, S. Zeytinolu, A. Abdumalikov, S. Berger, A. Wallraff, and S. Filipp, Microwave-Controlled Generation of Shaped Single Photons in Circuit Quantum Electrodynamics, *Phys. Rev. X* **4** (2014).
- [41] P. Kurpiers, P. Magnard, T. Walter, B. Royer, M. Pechal, J. Heinsoo, Y. Salath, A. Akin, S. Storz, J.-C. Besse *et al.*, Deterministic quantum state transfer and remote entanglement using microwave photons, *Nature (London)* **558**, 264 (2018).
- [42] S. Rosenblum, Y. Y. Gao, P. Reinhold, C. Wang, C. J. Axline, L. Frunzio, S. M. Girvin, L. Jiang, M. Mirrahimi, M. H. Devoret *et al.*, A CNOT gate between multiphoton qubits encoded in two cavities, *Nat. Commun.* **9**, 652 (2018).
- [43] P. Magnard, P. Kurpiers, B. Royer, T. Walter, J.-C. Besse, S. Gasparinetti, M. Pechal, J. Heinsoo, S. Storz, A. Blais *et al.*, Fast and Unconditional All-Microwave Reset of a Superconducting Qubit, *Phys. Rev. Lett.* **121**, 060502 (2018).
- [44] X. Jin, A. Kamal, A. Sears, T. Gudmundsen, D. Hover, J. Miloshi, R. Slattery, F. Yan, J. Yoder, T. Orlando *et al.*, Thermal and Residual Excited-State Population in a 3D Transmon Qubit, *Phys. Rev. Lett.* **114**, 240501 (2015).
- [45] K. Serniak, M. Hays, G. de Lange, S. Diamond, S. Shankar, L. Burkhardt, L. Frunzio, M. Houzet, and M. Devoret, Hot Nonequilibrium Quasiparticles in Transmon Qubits, *Phys. Rev. Lett.* **121**, 157701 (2018).
- [46] B. G. Christensen, C. D. Wilen, A. Opremcak, J. Nelson, F. Schlenker, C. H. Zimonick, L. Faoro, L. B. Ioffe, Y. J. Rosen, J. L. DuBois *et al.*, Anomalous charge noise in superconducting qubit, *Phys. Rev. B* **100** (2019).
- [47] A. P. Vepsilinen, A. H. Karamlou, J. L. Orrell, A. S. Dogra, B. Loer, F. Vasconcelos, D. K. Kim, A. J. Melville, B. M. Niedzielski, J. L. Yoder *et al.*, Impact of ionizing radiation on superconducting qubit coherence, *Nature (London)* **584**, 551 (2020).
- [48] R.-P. Riwar, A. Hosseinkhani, L. D. Burkhardt, Y. Y. Gao, R. J. Schoelkopf, L. I. Glazman, and G. Catelani, Normal-metal quasiparticle traps for superconducting qubits, *Phys. Rev. B* **94** (2016).
- [49] J.-H. Yeh, J. LeFebvre, S. Premaratne, F. C. Wellstood, and B. S. Palmer, Microwave attenuators for use with quantum devices below 100 mK, *J. Appl. Phys.* **121**, 224501 (2017).
- [50] Z. Wang, S. Shankar, Z. Mineev, P. Campagne-Ibarcq, A. Narla, and M. Devoret, Cavity Attenuators for Superconducting Qubits, *Phys. Rev. Applied* **11**, 014031 (2019).
- [51] J. Conrad, O. Botner, A. Hallgren, and C. Prez de los Heros, Including systematic uncertainties in confidence interval construction for Poisson statistics, *Phys. Rev. D* **67** (2003).
- [52] W. A. Rolke, A. M. Lpez, and J. Conrad, Limits and confidence intervals in the presence of nuisance parameters, *Nucl. Instrum. Methods Phys. Res., Sect. A* **551**, 493 (2005).
- [53] J. W. Foster, N. L. Rodd, and B. R. Safdi, Revealing the dark matter halo with axion direct detection, *Phys. Rev. D* **97** (2018).
- [54] J. Gambetta, A. Blais, D. I. Schuster, A. Wallraff, L. Frunzio, J. Majer, M. H. Devoret, S. M. Girvin, and R. J. Schoelkopf, Qubit-photon interactions in a cavity: Measurement-induced dephasing and number splitting, *Phys. Rev. A* **74**, 042318 (2006).
- [55] S. D. McDermott and S. J. Witte, Cosmological evolution of light dark photon dark matter, *Phys. Rev. D* **101**, 063030 (2020).
- [56] A. P. M. Place, L. V. H. Rodgers, P. Mundada, B. M. Smitham, M. Fitzpatrick, Z. Leng, A. Premkumar, J. Bryon, S. Sussman, G. Cheng *et al.*, New material platform for superconducting transmon qubits with coherence times exceeding 0.3 milliseconds, [arXiv:2003.00024](https://arxiv.org/abs/2003.00024).
- [57] D. Alesini, C. Braggio, G. Carugno, N. Crescini, D. D'Agostino, D. Di Gioacchino, R. Di Vora, P. Falferi, U. Gambardella, C. Gatti *et al.*, High quality factor photonic cavity for dark matter axion searches, *Rev. Sci. Instrum.* **91**, 094701 (2020).
- [58] D. McClure, H. Paik, L. Bishop, M. Steffen, J. M. Chow, and J. M. Gambetta, Rapid Driven Reset of a Qubit Readout Resonator, *Phys. Rev. Applied* **5**, 011001 (2016).
- [59] T. Walter, P. Kurpiers, S. Gasparinetti, P. Magnard, A. Potonik, Y. Salath, M. Pechal, M. Mondal, M. Oppliger, C. Eichler *et al.*, Rapid High-Fidelity Single-Shot Dispersive Readout of Superconducting Qubits, *Phys. Rev. Applied* **7**, 054020 (2017).
- [60] N. Leung, Y. Lu, S. Chakram, R. Naik, N. Earnest, R. Ma, K. Jacobs, A. Cleland, and D. Schuster, Deterministic bidirectional communication and remote entanglement generation between superconducting quantum processors, *npj Quantum Inf.* **5** (2018).
- [61] C. J. Axline, L. D. Burkhardt, W. Pfaff, M. Zhang, K. Chou, P. Campagne-Ibarcq, P. Reinhold, L. Frunzio, S. M. Girvin, L. Jiang *et al.*, On-demand quantum state transfer and entanglement between remote microwave cavity memories, *Nat. Phys.* **14**, 705 (2018).
- [62] S. Chakram, K. He, A. V. Dixit, A. E. Oriani, R. K. Naik, N. Leung, H. Kwon, W.-L. Ma, L. Jiang, and D. I. Schuster, Multimode photon blockade, [arXiv:2010.15292](https://arxiv.org/abs/2010.15292).
- [63] R. K. Naik, N. Leung, S. Chakram, P. Groszkowski, Y. Lu, N. Earnest, D. C. McKay, J. Koch, and D. I. Schuster, Random access quantum information processors using multimode circuit quantum electrodynamics, *Nat. Commun.* **8** (2017).
- [64] Y. Y. Gao, B. J. Lester, Y. Zhang, C. Wang, S. Rosenblum, L. Frunzio, L. Jiang, S. M. Girvin, and R. J. Schoelkopf, Programmable Interference between Two Microwave Quantum Memories, *Phys. Rev. X* **8**, 021073 (2018).